NURETH14-277

THE EFFECT OF BINARY OXIDE MATERIALS ON A SINGLE DROPLET VAPOR EXPLOSION TRIGGERING

R. C. Hansson[1], L. T. Manickam[1] and T. N. Dinh[1]
[1] Royal Institute of Technology, Stockholm, Sweden

Abstract

In order to explore the fundamental mechanism dictated by the material influence on triggering, fine fragmentation and subsequent vapor explosion energetics, a series of experiments using a mixture of eutectic and non-eutectic binary oxide were initiated. Dynamics of the hot liquid (WO_3-CaO) droplet and the volatile liquid (water) were investigated in the MISTEE (Micro-Interactions in Steam Explosion Experiments) facility by performing well-controlled, externally triggered, single-droplet experiments, using a high-speed visualization system with synchronized digital cinematography and continuous X-ray radiography, called SHARP (Simultaneous High-speed Acquisition of X-ray Radiography and Photography). The acquired images followed by further analysis showed a milder interaction for the non-eutectic melt composition for the tests with low melt superheat, whether no evident differences between eutectic and non-eutectic melt compositions regarding bubble dynamics, energetics and melt preconditioning was perceived for the high melt superheat tests.

Introduction

Motivated by the risk assessment of a steam explosion in light water reactors, in the last decades much work has been done with the purpose of developing a better understanding on the thermo-hydraulic processes that govern the phenomenon. Large and intermediate scale experiments have shown, however, mixed results on the triggability and explosion yield of various molten materials (from pure metallic and oxidic melts to prototypic corium melts). Generally speaking, metallic and alumina melts were shown to be prone to energetic steam explosions, whether binary and multi-component melts exhibited a low disposition for such interaction.

ZrO_2 and Al_2O_3 were the most accepted single component simulants of corium used for inducing steam explosions.

In experiments involving Zr/ZrO_2 and Zr/SS [1, 2], spontaneous explosions were observed in high subcooled coolant conditions, and the explosion energy significantly increased with increasing content of zirconium in the melt. The energetics is believed to be augmented by the zirconium-water chemical reaction, which would be dependent on the zirconium concentration in the melt. However, it was not possible to distinguish between the relative contributions of thermal and chemical energy to the overall explosion work, leaving an open question about the likelihood of the chemical energy release and conversion into mechanical work.

Alumina, usually prepared by a termite reaction with iron oxide, generated energetic spontaneous steam explosions when poured in subcooled water, independent of its superheat. Experiments using near saturated water pools suppressed the spontaneity of the explosions, although given an initial trigger an energetic interaction took place. [3, 4, 5, 6]

Alumina exhibits certain peculiarities in thermal conductivity (~3 times higher than corium), emissivity (semi-transparent characteristic) [7], as well as chemical stability (formation of gamma- alumina) [8], that might explain its explosive behavior specially when compared to corium. In addition, alumina creates a different premixing trait due to the hydrodynamic fragmentation characteristic of the jet during its pouring into the water, i.e. its low density leads to the formation of larger droplets which in turn produces a less voided premixture. All these aspects make it difficult to pinpoint the actual material effect on steam explosion triggering and energetics.

More recently, in corium experiments with eutectic and non-eutectic mixtures, it was observed that the eutectic corium exploded spontaneously whereas the non-eutectic corium was found to be resilient to an energetic interaction even when the FCI (Fuel-Coolant Interaction) pre-mixture was triggered. In the TROI tests series, more than 10 experiments using UO_2-ZrO_2 at a non-eutectic 80:20 composition hardly lead to an energetic steam explosion, while four tests resulted in spontaneous steam explosions among the six experiments using eutectic corium at 70:30 [9, 10].

Because the thermo-physical properties of the non-eutectic corium at 80:20 composition would be different within an order of 10% from those of an eutectic corium at 70:30 composition, the premixing behavior is not expected to be different between the two types of corium, since the initial and boundary conditions for the fuel-coolant-interaction tests are very similar. Thus, it is highly probable that other material properties rather than the thermo-physical properties are the reason for the difference in steam explosion behavior. Solidification characteristics of the eutectic and non-eutectic materials could be the fundamental mechanism responsible for such disparity.

Based on the particular solidification characteristics of binary oxides, Okkonen *et al.* [11], Dinh [12] and Haraldsson [13] proposed that, when dealing with concentrations away from the eutectic point, a mushy layer will be formed on the droplet surface. Such mushy phase would significantly increase the viscosity and effective surface tension, rendering the droplet's resilience to external forcing, including disturbances due to local melt-coolant contacts.

Min *et al*. [14] performed physical and chemical analyses on the solidified UO_2-ZrO_2 debris from six TROI tests. It was found that non-eutectic quenched particles showed cracks, possibly due to volume shrinkage during solidification, while the eutectic UO_2-ZrO_2 had big pores inside the debris particles. These differences reinforce the existence of different solidification behavior between eutectic material and non-eutectic material. For the non-eutectic mixture, the solid nuclei in the mushy phase would become nucleation sites, resulting in a uniform solidification if the nuclei population is high. Conversely, in the eutectic material the core part of the particle remains as liquid, while the surface layer solidifies. It would have much fewer number of

nucleation sites. As a result, the tension between the liquid in the core and the solidified surface layer leads to the formation of many pores in the particle.

Song *et al*. [15] analyzed the debris of the TROI experiments using partially oxidized corium and proposed that the inner porous structure of the particles, similar to the one observed by Min *et al*., would affect the fine fragmentation behavior during propagation of an explosion, since a considerable amount of droplets would be at similar heterogeneous mixture state, i.e. solid and liquid, during the FCI process before solidifying.

Dinh [16], argued that the mushy zone phase would not be active during the premixing phase, as the time window for the mushy phase to exist on the droplet surface is small compared to the premixing time. Therefore, the effects of the melt's non-eutectic composition should be sought in the fine fragmentation during the explosion phase.

Bearing in mind such time scale, the extent of the proposed melt preconditioning [17] would be a reflection of the so discussed mushy zone, i.e. its occurrence would directly influence the ability of the melt droplet to deform/prefragment. That is to say, a binary non-eutectic oxidic corium melt droplet can form a deformation-resistant mushy surface layer in a much shorter time than a droplet of molten alumina, steel or even eutectic corium, which will directly affect the steam explosion energetics.

In this paper, the role of the melt superheat and preconditioning will be investigated with the objective to elucidate the apparent difference between eutectic and non-eutectic materials on the steam explosion energetics.

1. Facility description

The test facility named MISTEE (**M**icro **I**nteractions in **S**team **E**xplosion **E**xperiments) shown in Fig. 1 is designed for the visualization of the explosion of a single droplet disturbed by a weak pressure wave, characteristic of the early triggering phase in a vapor explosion. The facility consists of a test chamber, a melt generator, an external trigger system, an operational control system, and a data acquisition and visualization system.

The test section is a rectangular Plexiglas tank (180×130×250mm) in which a piezoelectric pressure transducer is flush-mounted at the center of the test section wall. A K-type thermocouple is employed to measure the water temperature inside the test section, and a C-type thermocouple is used to measure the molten droplet temperature in the furnace. The melt generator consists of an induction furnace (260V, 40A) and a graphite cylinder (40mm O.D. × 50mm) with a molybdenum crucible (20mm I.D. × 30mm). A molten WO_3-CaO mass of ~1g is loaded to the crucible to guarantee the single-droplet delivery through a 5.0mm hole at the center of the crucible bottom. The melt generator, which includes the induction coil and crucible, is housed inside a chamber into which argon gas is purged in to suppress the thermocouple oxidation and burning of the graphite crucible during the heating and melting phases. A tungsten plug is used to block the hole in the crucible bottom during the melting and this plug is lifted by a pneumatic piston to release the melt droplet. The external trigger system can be described as a piston located at the bottom of the test section, which generates the sharp pressure pulse (rising

time of 50 μs at the full width half maximum) up to 0.15 MPa that travels through the coolant. The trigger hammer that impacts on the piston to generate a pressure pulse is aligned underneath the latter, and is driven by a rapid discharge of a capacitor bank, consisting of three capacitors of 400 Vdc and 4700 mF each.

The fast synchronous visualization system, **SHARP** (**S**imultaneous **H**igh-speed **A**cquisition of x-ray **R**adiography and **P**hotography), consists of tungsten lighting and a high speed CMOS digital camera (Redlake HG50LE), up to 100000 fps (with 20000 fps rate used in the actual tests) for the photography; and a continuous X-ray source tube (Philips MCN 321 - max. 320 keV), an X-ray converter and an image intensifier coupled to a high speed camera (Lightning RDT^{Plus} camera), for radiographic imaging up to 50000 fps (with 5000 fps rate used in the actual tests). Image processing methods were developed to process and synchronize the photographic and X-ray radiographic images [18].

A more detailed description of the equipment, test procedure, assessment of measurement uncertainty and image processing methods can be found elsewhere [19].

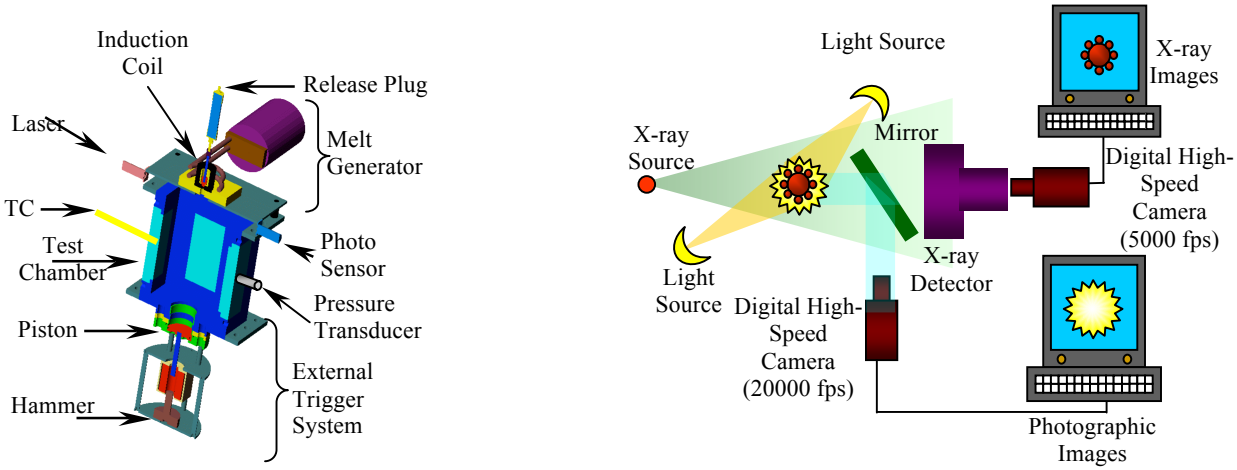

Figure 1 MISTEE test section and SHARP visualization system.

2. MISTEE binary oxide single droplet experiments

Two series of externally triggered single-drop experiments, in which WO_3-CaO was used as the melt material and water as coolant, were performed on the MISTEE test facility. In the first test series, experiments with an eutectic composition (75:25 mol%, $T_{liquidus}$=1135°C,) and with a non-eutectic composition (72:27 mol%, $T_{liquidus}$=1232°C, $T_{solidus}$=1135°C) of WO_3-CaO, were performed under high subcooled coolant conditions (~20°C) and high initial melt superheat ($\Delta T_{superheat}$~200°C to 300°C[1]). In the second test series, similar water subcooling and melt

[1] Measured in the crucible before the melt discharge into the water tank.

compositions, i.e. eutectic and non-eutectic WO_3-CaO, were employed; the melt superheat, however, was lower (~100°C) than the first test series.

From both series a number of tests were chosen for the actual analysis due to their data completeness, i.e. simultaneous record of bubble and melt dynamics.

Still photographic images, with a temporal resolution of 0.05 ms per frame and the corresponding X-ray radiography images, with a temporal resolution of 0.2 ms per frame, are presented in Figures 2 to 5. The images reveal the vapor film and melt progression during the steam explosion of ~1 g of eutectic and non-eutectic molten WO_3-CaO droplet under high water subcooling, and different melt superheat.

Similar to the single droplet experiments performed with a metallic melt (tin) [17], the vapor film dynamics produces three defined cycles of bubble expansion and collapse, as seen in Figure 6. For convenience, we define t=0 ms at the final collapse of the first vapor bubble's cycle.

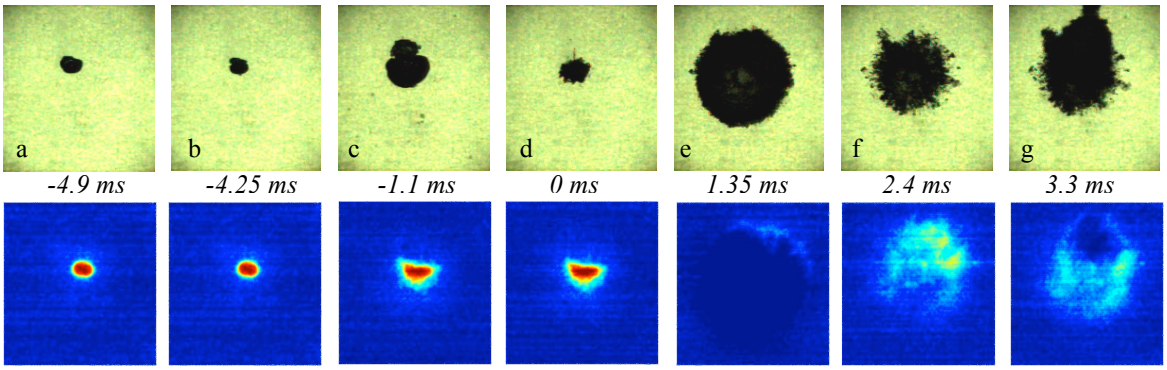

Figure 2 Vapor film (top) and melt dynamics (bottom) of a single droplet of eutectic WO_3-CaO initially at 1350°C superheat, undergoing vapor explosion in water at 20.4°C.

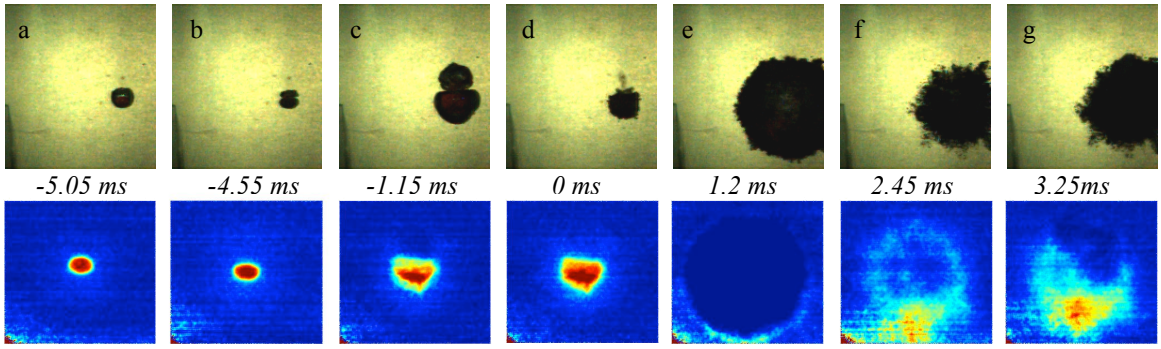

Figure 3 Vapor film (top) and melt dynamics (bottom) of a single droplet of non-eutectic WO_3-CaO initially at 1480°C superheat, undergoing vapor explosion in water at 20.1°C.

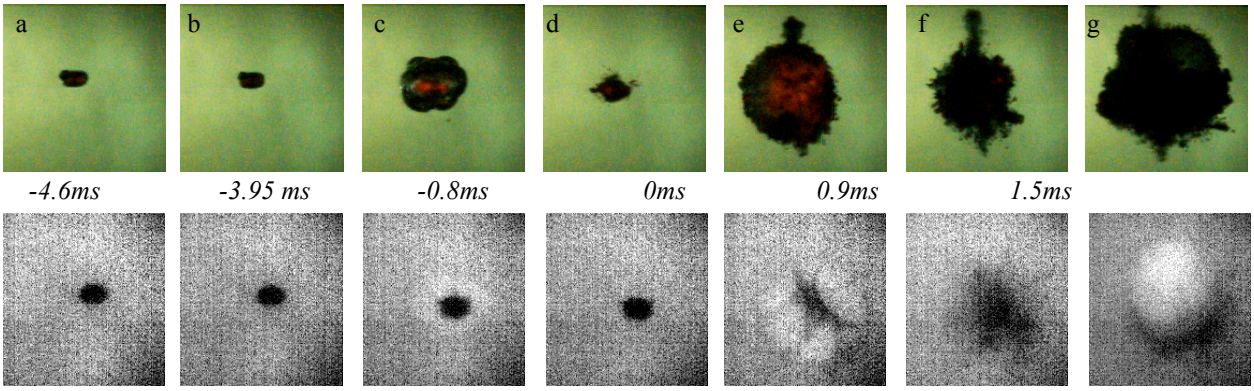

Figure 4 Vapor film (top) and melt dynamics (bottom) of a single droplet of eutectic WO_3-CaO initially at 1251°C superheat, undergoing vapor explosion in water at 23°C.

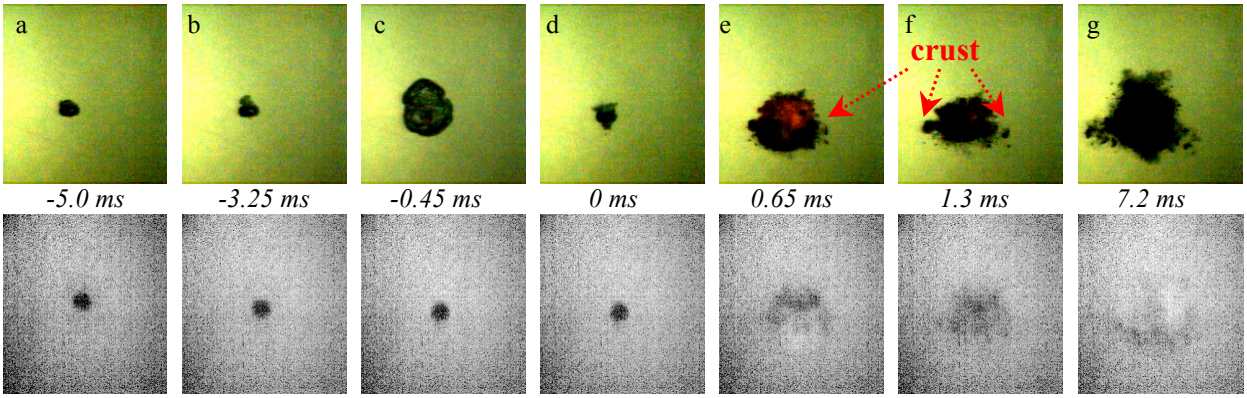

Figure 5 Vapor film (top) and melt dynamics (bottom) of a single droplet of non-eutectic WO_3-CaO initially at 1350°C superheat, undergoing vapor explosion in water at 22.3°C.

Due to the melt's high temperature, a vapor film with a small dome on the rear side is immediately formed at the time the molten WO_3-CaO droplet enters the water, and endures as it descends into the test section, Fig. 2-5a, with a velocity of approximately 0.47m/s. The interaction is initiated once the external pressure wave destabilizes the vapor film, Fig. 2-5b, triggering the parallel oscillatory behavior of the bubble/ rear and cyclic jet formation underneath of the main bubble. Melt-coolant local contacts occur and subsequent nucleation takes place initiating the bubble's *first cycle* expansion. During this cycle, the vapor film dynamics creates complex internal flows that disturb the melt droplet surface facilitating its deformation/prefragmentation, i.e. preconditioning. That can be clearly seen in the radiographic images, in which the initial elliptical droplet, Fig 2-5a (bottom), evolves into a convoluted droplet with fine fragments present in the droplet's periphery, Fig 2-5c (bottom).

The overgrown bubble/rear reaches its maximum, Fig 2-5c, and starts to collapse towards the molten droplet. The accelerating interface hits the molten droplet, adding the coolant into the interaction zone. At this point (t=0 ms), the actual direct melt-coolant mixing takes place, Fig 2-5d, which leads to the bubble's *second cycle* characterized by the explosive evaporation and fine fragmentation of the melt droplet. The produced fine fragments set off in the radial direction

following the interface of the growing bubble, forming a shell-like region of finely fragmented melt particles. As the vapor bubble decelerates, the inertia continues to drive the fine fragments to penetrate deeper into the liquid domain. The bubble reaches its maximum size, Fig 2-5e, and subsequently collapses, leaving the fine fragments behind whereas a fraction of them is redistributed in the center region of the original droplet. At this point, the bubble dynamics cannot be precisely discerned since the cloud of fine fragments unable the exact resolution of the vapor interface. Nevertheless, the bubble's *third cycle* can still be recognized, when the collapsing bubble promotes the mixing of the coolant and the remains of the molten material, Fig 2-5f, leading to a secondary explosive vaporization, Fig 2-5g. The fine fragments are then dispersed within the coolant after the bubble has finally collapsed.

No apparent dissimilarities in the vapor film and melt dynamics were found for the test series under high melt superheat (Fig. 2 and 3): both melt compositions, i.e. eutectic and non-eutectic WO_3-CaO, consistently led to explosive vapor generation and subsequent fine fragmentation of the droplet in three cycles. Conversely, the test series with non-eutectic WO_3-CaO under lower melt superheat (Fig. 5) reveal the presence of portions of a crust on the second cycle during fragmentation, Fig 5e-f, whether the eutectic tests (Fig. 4) regularly led to the fine fragmentation of melt droplet similar to the high superheat tests.

Differences in melt fragmentation will directly influence the vapor explosion energetics, since it is an indication of the amount of melt involved in the interaction, besides defining the heat transfer area. Accordingly, one should expect a milder interaction in the low superheat non-eutectic experiments, given that the fine fragmentation is diminutive.

The equivalent diameter[2], normalized by its value prior to the external disturbance, is shown in Figure 6 for eutectic (e) and non-eutectic (ne) mixtures of WO_3.-CaO and different melt superheat. One can clearly identify the three cycles mentioned previously. In the high melt superheat tests, Fig. 6a, both melt compositions cover a wide spectrum of the vapor film history and no particularity can be discerned. The lower melt superheat tests, Fig. 6b, appear to show a tendency of a more pronounced 2^{nd} and 3^{rd} cycle in the eutectic runs; however a clearer picture of such differences should arise by evaluating the energetics associated with the interaction.

The melt preconditioning (deformation/pre-fragmentation of a molten droplet during the first bubble cycle), postulated to dictate the interaction's conversion ratio [17], is quantified by the droplet's projected area evolution depicted in the radiographic images.

Figure 7a points out to no apparent differences between the eutectic and non-eutectic tests with high melt superheat in terms of steam explosion energetics and preconditioning, which is a reflection of what is seen in the bubble dynamics, Fig. 6a. In contrast, Figure 7b shows a divergence between the energetics and melt preconditioning of the eutectic and non-eutectic tests, i.e. non-eutectic test led to a milder interaction than the eutectic tests.

[2] Estimated from the vapor bubble projected area.

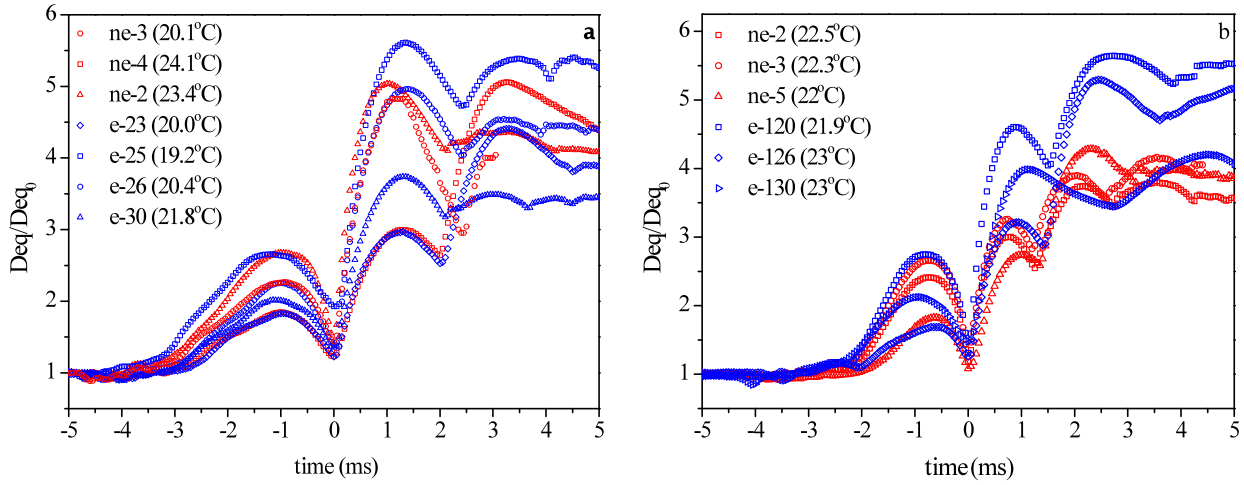

Figure 6 Radial history of eutectic (e) and non-eutectic (ne) WO3-CaO single droplet for high (a) and low (b) melt superheat, with the respective water temperature.

Such observations can be rationalized by considering the phase change of a non-eutectic binary oxidic melt droplet, i.e. solidification and/or formation of a mushy phase, which typically occurs over a specific temperature range determined by the *liquidus* and *solidus* line. Accordingly, if the droplet superheat is high enough the material phase will be kept far above the liquidus line, i.e. in liquid form, during the interaction for both melt compositions. That is to say, that the melt droplet will be away from the region in which solidification behaviors would play a role on the melt preconditioning and thus in the steam explosion energetics, Fig 7a.

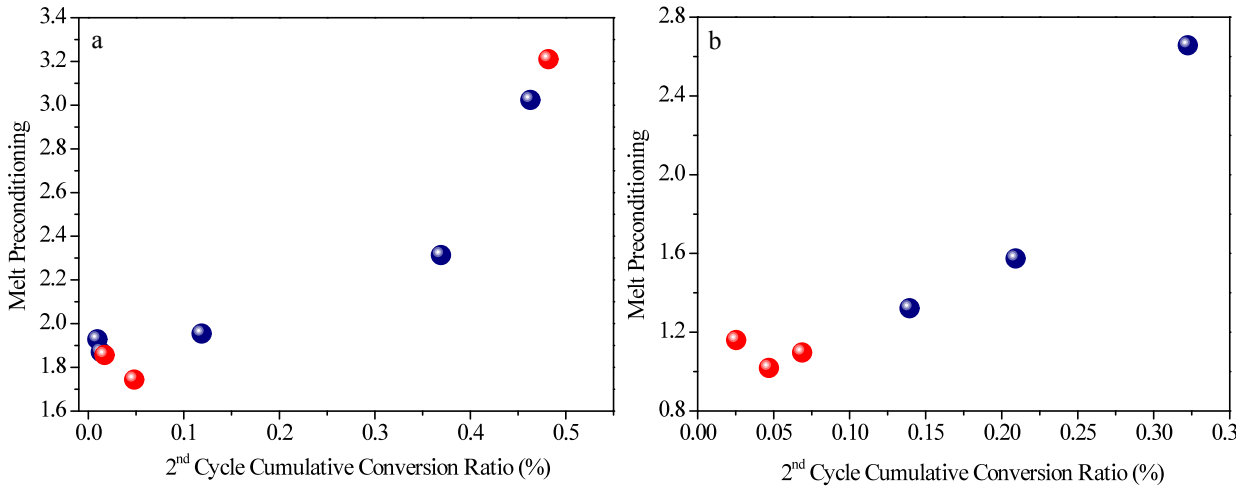

Figure 7 Melt droplet preconditioning and 2nd cycle cumulative conversion ratio of eutectic (blue) and non-eutectic (red) WO3-CaO single droplet for high (a) and low (b) melt superheat.

Then again, in the case of low superheat experiments, the melt temperature falls into such specific temperature range, i.e. between the liquidus and solidus line for the non-eutectic material, which can be augmented by the difference in undercooling characteristic of such fast

quenching (direct melt-coolant contact) [16]. In fact, for non-eutectic materials, it suffices to remove only a fraction of the latent heat of fusion to bring the melt into a mushy state.

Once in this regime, formation of a thin crust or even a mushy layer on the droplet's surface would significantly increase the viscosity and effective surface tension, rendering the droplet resilience to external forcing, including external disturbances due to local melt-coolant contacts. Correspondingly, the non-eutectic WO_3-CaO melt droplet shows a diminutive melt preconditioning due to such deformation resistant state, which then reflects on the vapor explosion conversion ratio, Fig 7b. Moreover, the consistent presence of a crust, Fig 5e-g, on the non-eutectic tests implies less melt material available for the interaction, contributing to the differences in energetics between eutectic and non-eutectic tests.

3. Discussions

Single droplet vapor explosion experiments with different compositions of WO_3-CaO were conducted in the MISTEE facility with the purpose to elucidate the effect of a binary oxide material on the FCI energetics. A system of synchronized high speed digital cinematography and X-ray radiography, named SHARP, is used to visualize and characterize the evolution and coupled dynamics of the vapor film and molten material, providing the data necessary for the analysis.

Estimated energetics points out to a milder interaction for the non-eutectic melt composition in the low superheat tests, particularly when compared to the tests with the melt droplet in a eutectic composition. Moreover, a thin crust was observed in the non-eutectic interaction during the explosive 2nd cycle. Such differences could not be perceived in the tests with high melt superheat, which consistently led to the fine fragmentation of the melt droplet.

The MISTEE data on the melt preconditioning (melt droplet deformation/prefragmentation established during the bubble's 1st cycle) confirm its direct relation to the interaction's conversion ratio, and implicate the governing role of the melt material on the triggering of a single droplet (binary oxide) vapor explosion. Namely, the distinction between eutectic and non-eutectic WO_3-CaO in the actual tests lies on the solidification characteristics of the melt droplet during the direct melt-coolant contact. However, the material effect of a binary oxide on the vapor explosion energetics can only be perceived when the melt droplet is in a quite specific temperature range, raising a question of its actuality on a large scale vapor explosion.

4. References

[1] D. H. Cho, D. R. Armstrong, W. H. Gunther, 'Experiments on interactions between zirconium-containing melt and water (ZREX): Hydrogen generation and chemical augmentation", JAERI-Conf 97-011, 1998.

[2] J. H. Song, I. K. Park, Y. J. Chang, Y. S. Shin, J. H. Kim, B. T. Min, S. W. Hong, H. D. Kim, "Experiments on the interactions of molten ZrO_2 with water using TROI facility", *Nuclear Engineering and Design*, Vol. 213 (2-3), 2002.

[3] N. Yamano, Y. Maruyama, T. Kudo, A. Hidaka, J. Sugimoto, "Phenomenological studies on melt-coolant interactions in the ALPHA program", *Nuclear Engineering and Design*, Vol. 155, 1995.

[4] L. D. Buxton, W. B. Benedick, "Steam explosion efficiency studies", *NUREG/CR-0947* (SAND-79-1399), 1978.

[5] I. Huhtiniemi, D. Magallon, and H. Hohmann, "Results of recent KROTOS FCI tests: alumina vs. corium melts", *Nuclear Engineering and Design*, Vol. 189, 1997.

[6] W. Cherdron, F. Huber, A. Kaiser, W. Schutz, "Eco steam explosion experiments: documentation and evaluation of experimental data", Wissenschaftliche Berichte FZKA, Vol. 7011, 2005.

[7] L. A. Dombrovsky, T. N. Dinh, "The effect of thermal radiation on the solidification dynamics of metal oxide melt droplets", *Nuclear Engineering and Design*, Vol. 238, 2008.

[8] P. Piluso, G. Trillon, D. Magallon, "Material effect and steam explosion at high temperature (T>2300K)", *International Journal of Thermophysics,* Vol 26, No. 4, 2005.

[9] J. H. Song, I. K. Park, Y. S. Shin, J. H. Kim, B. T. Min, S. W. Hong, H. D. Kim, "Fuel coolant interaction experiments in TROI using a UO2/ZrO2 mixture", *Nuclear Engineering and Design*, Vol. 222, 2003.

[10] J. H. Song, S. B. Kim, H. D. Kim, "On some salient unresolved issues in severe accidents for advanced light water reactors", *Nuclear Engineering and Design*, Vol. 235(17-19), 2005.

[11] T. Okkonen and B. R. Sehgal, "Experiments on melt droplets falling into a water pool", JAERI-Conf 97-011, 1997.

[12] T. N. Dinh, A. T. Dinh, J. A. Green, B. R. Sehgal, "An assessment of steam explosion potential in molten-fuel-coolant interaction experiments", Proceedings International Conference on Nuclear Engineering (ICONE-6), San Diego, USA, May 1998.

[13] H. O. Haraldsson, "Breakup of jet and drops during premixing phase of fuel coolant interactions", Doctoral Thesis, Royal Institute of Technology, 2000.

[14] B. T. Min, J. H. Song, Y. S. Park, J. G. Kim, "A physical and chemical analysis of fast quenched particles of UO_2 and ZrO_2 mixture", *Journal of Nuclear Materials,* Vol. 358, 2006.

[15] J. H. Song, B. T. Min, F. Defoort, "The effect of material composition on the strength of a steam explosion", *Heat Transfer Engineering,* Vol. 29(8), 2008.

[16] T. N. Dinh, "Material property effect in steam explosion energetics: revisited", NURETH-12, Pennsylvania, USA, September 30-October 4, 2007.

[17] R. C. Hansson, T. N. Dinh, H. S. Park, "Dynamics and preconditioning in a single droplet vapor explosion", *Nuclear Technology*, Vol. 167, 2008.

[18] R. C. Hansson, T. N. Dinh, H. S. Park, "Simultaneous High Speed Digital

Cinematographic and X-ray Radiographic Imaging of an Intense Multi-Fluid Interaction with Rapid Phase Changes", *Experimental Thermal and Fluid Sciences,* Vol. 33, 2009.